Geophysical Research Letters

RESEARCH LETTER
10.1029/2019GL082999

Along-Slope Variability of Cross-Slope Eddy Transport in East Antarctica

Annie Foppert[1,2], **Stephen R. Rintoul**[1,2,3], **and Matthew H. England**[4,5]

[1]Centre for Southern Hemisphere Oceans Research, Hobart, Tasmania, Australia, [2]CSIRO Oceans and Atmosphere, Hobart, Tasmania, Australia, [3]Antarctic Climate and Ecosystems Cooperative Research Centre, Hobart, Tasmania, Australia, [4]Climate Change Research Centre, University of New South Wales, Sydney, New South Wales, Australia, [5]ARC Centre of Excellence for Climate Extremes, University of New South Wales, Sydney, New South Wales, Australia

Key Points:
- Cross-slope eddy transport is inferred from observed density-layer thickness gradients in East Antarctica between 0°E and 160°E
- Enhanced onshore transport (≈1.5 × East Antarctic mean) of warm, salty Circumpolar Deep Water occurs in regions of high isopycnal spice variability
- Eddy-induced overturning carries ≈0.8 m^2/s of CDW poleward to produce warm, salty anomalies at the shelf break in eddying regions

Correspondence to:
A. Foppert,
annie.foppert@csiro.au

Citation:
Foppert, A., Rintoul, S. R., & England, M. H. (2019). Along-slope variability of cross-slope eddy transport in East Antarctica. *Geophysical Research Letters*, *46*, 8224–8233. https://doi.org/10.1029/2019GL082999

Received 25 MAR 2019
Accepted 11 JUL 2019
Published online 24 JUL 2019

Abstract Circumpolar Deep Water (CDW) transport across the Antarctic continental slope regulates the delivery of heat to the shelf and its availability to melt floating ice shelves. The cross-slope density field, calculated from profiles collected by conductivity-temperature-depth-tagged marine mammals on the East Antarctic slope (0–160°E, above 1,000- to 3,000-m isobaths), indicates eddy-driven overturning: onshore transport of CDW and offshore transport of shallower Antarctic Surface Water. Enhanced eddy activity, determined by a spice standard deviation threshold in the CDW layer, is present over about a third of the East Antarctic slope analyzed. Significantly stronger CDW transport in regions of elevated spice variability produces subsurface temperature anomalies of 0.2–0.25 °C relative to the East Antarctic average. Estimating eddy diffusivity from the hydrography yields about 0.8 m^2/s of warm CDW transport to the shelf break in high-variability regions. Variability of eddy-induced CDW transport influences the reservoir of heat available for transport across the shelf break.

Plain Language Summary The transport of warm water from the open ocean to the Antarctic continental shelf has global significance, as it regulates the melt of ice shelves and dense water formation. We quantify the strength of eddy-driven transport of relatively warm Circumpolar Deep Water (CDW) across the continental slope of East Antarctica from the observed cross-slope density structure. We find that, in general, there is an eddy-driven overturning: deeper CDW is transported onshore while shallower Antarctic Surface Water is transported offshore. Upon closer inspection, we find that regions with elevated temperature and salinity variability on density surfaces are associated with significantly stronger onshore transport of CDW by eddies. These hot spots of eddy transport produce warm and salty anomalies at the shelf break, impacting the reservoir of heat available to the shelf.

1. Introduction

The transport of relatively warm and salty Circumpolar Deep Water (CDW) across the Antarctic continental slope and onto the shelf controls the amount of heat available to melt floating ice shelves, thus influencing global mean sea level, and impacts the heat and salt budget in regions of bottom water formation, thus influencing global overturning circulation (Heywood et al., 2014). Around the Antarctic continental slope, CDW sits deeper and farther offshore than the colder and fresher Antarctic Surface Water (AASW), separated by the Antarctic Slope Front (ASF; Whitworth et al., 1998). In this way, the ASF acts as a gateway to the continental shelf—a region of water mass transformation and ocean-ice interaction (Thompson et al., 2018). Therefore, identifying and understanding the physical processes responsible for driving cross-slope CDW transport has global significance.

Poleward transport of CDW across the slope is achieved by different processes, including eddies and mean flows (Heywood et al., 2014). Observational (Nøst et al., 2011; Thompson et al., 2014) and modeling (Palóczy et al., 2018; Stewart et al., 2018) studies have recently demonstrated the importance of eddies in driving cross-slope exchange and poleward heat transport. Ultrahigh resolution model results show the relative importance of eddy transport increases in deeper waters (approximately above the 1,000- to 3,500-m isobaths) and that the strength of the eddy transport varies with longitude (Stewart et al., 2018). Assuming that eddies tend to homogenize potential vorticity, the direction of eddy transport can be directly inferred from cross-slope changes in mean density-layer thickness (Karsten & Marshall, 2002; Marshall & Radko, 2003).

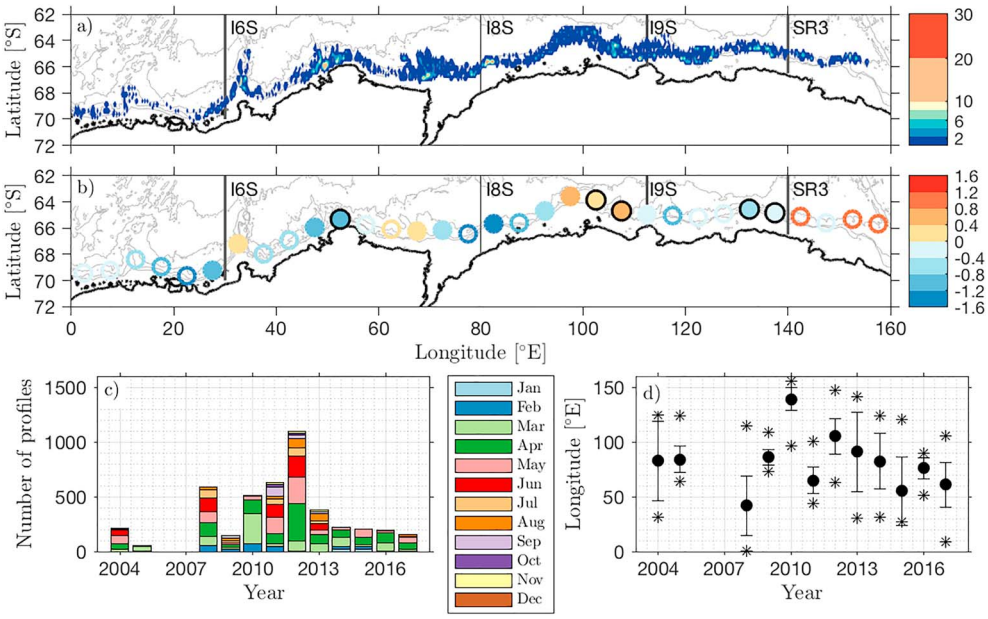

Figure 1. (a) Distribution of marine mammal-based conductivity-temperature-depth profiles along the East Antarctic continental slope. Colors represent the number of profiles recorded in each 0.25° × 0.25° region on the slope. Bathymetry is contoured every 1,000 m in gray and the coast is shown by the thick black contour. (b) Mean temperature, $\bar{T}$ (°C), at 300 dbar within 5° longitude bins between 0°E and 160°E and above the 1,000- to 3,000-m isobaths. Bathymetry is plotted as in panel (a). Longitudinal bins excluded from the analysis due to data sparsity are represented by unfilled circles; temperature values that fall in regions of high variability are outlined in black. (c) Temporal distribution of profiles with colors representing the month of year. (d) Longitudinal distribution of profiles for each year. Filled circles represent the mean longitude, error bars represent the standard deviation, and stars represent the minimum and maximum longitude.

The magnitude of eddy transport can then be calculated as $\psi_{\text{eddy}} = \overline{v'h'} = -\kappa \bar{h}_y$, where κ is an eddy diffusivity and $\bar{h}_y$ is the mean thickness gradient in an isopycnal layer. Thompson et al. (2014) used this method on 3 months of high-resolution glider data from the northwest Weddell Sea and found the eddy-driven transport scales to about half the magnitude of the wind-driven transport, making eddies a key driver of the overturning circulation.

While most of the mass loss to date from Antarctic ice shelves and grounded ice has come from West Antarctica (IMBIE, 2018; Paolo et al., 2015), there is growing evidence that parts of East Antarctica are also undergoing rapid change. For example, thinning of the grounded ice at the Totten Glacier has been observed in satellite data (Flament & Rémy, 2012; Harig & Simons, 2015; Pritchard et al., 2009) and the grounding line has retreated (Li et al., 2015). Oceanographic observations in front of the Totten Ice Shelf confirm that inflow of warm water is driving rapid basal melt of the ice shelf (Rintoul et al., 2016). Given that East Antarctica holds a volume of marine-based ice that is 5 times larger than that found in West Antarctica (Fretwell et al., 2013), it is important to assess the potential vulnerability of the East Antarctic Ice Sheet to ocean heat flux. The harsh climate and remote location of the Antarctic slope region has made it chronically underobserved, especially given its out-sized global influence. In this study, we take advantage of the advent of micro-conductivity-temperature-depth (CTD) tags for marine mammals (Treasure et al., 2017) to provide a new perspective on the importance of eddies in transporting CDW across the continental slope. Eddy transport across the East Antarctic slope, inferred from cross-slope changes in the mean thickness of density layers, is estimated from available hydrography described in section 2 and its along-slope variability is presented in section 3. A discussion of the results puts this work into a broader context (section 4) and is followed by summarizing conclusion (section 5).

2. Data

2.1. Seal-Based Hydrography

Satellite-linked micro-CTDs have been tagged to marine mammals starting in 2004 and continuing through today (Roquet et al., 2014). CTD data are recorded as the seals resurface after foraging for food in the water

column. When the animal surfaces, the data are sent ashore via the ARGOS system, with geopositioning accuracy of about ±5 km (Roquet et al., 2014). This work uses the November 2017 release of the data set collected by the Marine Mammals Exploring the Oceans Pole to Pole consortium (Roquet et al., 2018). Along the East Antarctic continental slope, there are 4,417 profiles with temperature, salinity, pressure, and location data that pass quality control (Figure 1). The accuracies of the calibrated and postprocessed temperature and salinity are quoted as ±0.02 °C and ±0.03 psu, respectively (Treasure et al., 2017). Profiles taken before 2007 used older technology resulting in accuracies of ±0.1 °C and ±0.1 psu, but most of the profiles analyzed here were taken more recently than 2007 (Figure 1c). The average depth of the profiles is about 600 dbar and the deepest reaching profile samples to 1,830 dbar. The pressures at which data are provided vary among profiles, as the data are compressed for satellite transmission with a "broken-stick" method to retain the structure of the high-resolution in situ data (Boehme et al., 2009). For this analysis, each individual seal-based CTD profile is linearly interpolated to a common pressure grid with 5-dbar spacing.

The spatial and temporal distributions of seal-based CTD profiles from the slope is shown in Figure 1. The monthly distribution of slope profiles varies from year to year, but the majority of profiles were consistently recorded in the austral autumn, March through May (Figure 1c). There are roughly 300 profiles per year on average, except in 2006 and 2007 when there are none and in 2012 when there are over 1,100 profiles. Likewise, the longitudinal distribution of profiles varies depending on year, with most profiles generally found between 50°E and 130°E (Figure 1d). However, profiles from 2010 were clustered farther east near 140°E and profiles from 2008 generally sampled farther west near 40°E.

2.2. Ship-Based Hydrography

Results from the seal-based CTD analysis are compared with ship-based CTD profiles from the Antarctic continental slope. These profiles are mostly from repeat hydrography (WOCE, CLIVAR, and GO-SHIP) lines that extend onto the East Antarctic slope, that is, I6S, I8S, I9S, and SR3, with their nominal locations shown in Figures 1a and 1b. The analysis also includes data from the BROKE (Bindoff et al., 2000) and BROKE-West (Meijers et al., 2010) missions that surveyed the ASF at several different longitudes in 1996 and 2006, respectively, where they coincide with repeat hydrography transects. The ship-based hydrography has low temporal resolution, yet generally high spatial and vertical resolution, and the resulting data are of the highest quality with accuracies in temperature and salinity of ±0.001 °C and ±0.002 psu. In some transects mesoscale eddies were sampled and in others the lighter AASW density classes outcrop at the surface; these occupations are excluded from this analysis as interest lies in the mean potential density structure. Thus, three occupations of I6S (1996, 2006, and 2008), six occupations of I8S (1994, 1996, 2003, 2006, 2007, and 2016), three occupations of I9S (1994, 2004, and 2012), and eight occupations of SR3 (1993, 1994, 2007, 2008, 2011, 2013, 2015, and 2018) are included in our analysis. Due to the sea ice expansion over the slope, all the ship-based hydrography profiles are sampled in Austral summer or early spring, December–April.

2.3. Bathymetry

The 2-min gridded global bathymetry data available through the ETOPO2v2 database (National Geophysical Data Center, 2006) are used to assign a water column depth to each CTD profile. Water column depth acts as a metric for offshore distance, with profiles in deeper water farther from the shelf. The cross-slope direction, used to calculate gradients of density-layer thickness, is defined by the water depth.

3. Methods

We use hydrographic profiles to diagnose eddy transport across the East Antarctic continental slope (defined here as waters between the 1,000- and 3,000-m isobaths and between 0°E and 160°E). The direction of eddy transport is inferred from cross-slope changes in the mean thickness of potential density layers. In each density class, following residual-mean theory (Karsten & Marshall, 2002; Marshall & Radko, 2003), mean eddy thickness transport is proportional to $\bar{h}_y$, where $\bar{h}$ is the mean thickness of a surface-referenced potential density layer, y is the cross-slope direction, and the subscript represents a derivative. In this sense, cross-slope eddy transport is directed from thicker to thinner regions of each density layer such that the eddies tend to homogenize potential vorticity.

The analysis of the seal-based data is complicated by its spatial and temporal distribution (described in section 2.1 and shown in Figure 1). The thickness of the CDW and AASW layers, defined by surface-referenced potential density (ρ) values, is calculated for every profile. Temperature and salinity profiles, and thickness of isopycnal layers, are averaged along and across the continental slope in bins defined

by 5° of longitude and isobaths separated by 400 m in depth. Standard deviations are also calculated in these longitude-isobath bins. That is, for example, the mean and standard deviation are calculated for all profiles taken from 0–5°E and above the 1,000- to 1,400-m isobaths. We only consider longitude bins where at least five profiles sampled to the base of the CDW layer, $\rho = 1027.82$ kg/m^3, over the midslope (i.e., open circles in Figure 1b are excluded). Thus, our analysis covers 70° of longitude along the East Antarctic continental slope and includes 3,126 profiles (about 2,000 of which reach 500 dbar).

Standard errors of the mean thickness estimates are calculated as $\sigma_h/\sqrt{N_{\text{profiles}}}$, where σ_h is the standard deviation of layer thickness and N_{profiles} is the number of profiles in each density class for every longitude-isobath bin. The uncertainty in surface-referenced density is found to be 0.003 kg/m^3 in the upper-middle-water column (300–1,000 dbar) of reconstructed profiles south of the Southern ACC Front, when accounting for calibration and data compression (Siegelman et al., 2019). With an average stratification of about $\rho_z = 3\times10^{-4}$ kg/m^4, this corresponds to an uncertainty in the depth of an isopycnal of roughly 10 m. The direction of the East Antarctic mean cross-slope eddy transport, that is, the sign of $\bar{h}_y$, is calculated by averaging the thickness of the CDW and AASW layers across longitudes as a function of water column depth. The standard error, representing natural variability among profiles, is propagated by taking the square root of the sum of the squared errors in each longitudinal segment.

Spiciness is a measure of the variation of temperature and salinity along density surfaces, and its variability give a sense of the strength of local isopycnal mixing (Munk, 1981; Stommel, 1961; Veronis, 1972). Note that spice is a differential value, such that only its relative magnitude and the magnitude of its isopycnal variability are of interest (McDougall & Krzysik, 2015). Spice referenced to the surface is calculated for each individual seal-based profile using the Gibbs Seawater Oceanographic Toolbox (McDougall & Barker, 2011). Within each longitude-isobath bin, spice profiles are averaged and standard deviations are calculated in isopycnal coordinates. That is, spice values are interpolated onto an even density grid with 0.01 kg/m^3 resolution before averaging. Spice standard deviation (σ_{spice}) provides a metric for eddy activity, with increased isopycnal spice variability indicating increased eddy mixing. The relative strength of eddy-driven transport is compared between regions of high and low spice variability, where high and low are defined as above and below a threshold value of spice standard deviation.

The magnitude of eddy transport of CDW is estimated as $\psi_{\text{eddy}} = \overline{v'h'} = -\kappa\bar{h}_y$, where $\kappa = L_{\text{mix}}U$ is an eddy diffusivity based on mixing length. The mixing length is calculated following Naveira Garabato et al. (2011), with spice as a passive tracer, such that $L_{\text{mix}} = \sigma_{\text{spice}}/|\overline{\text{spice}}_y|$ in the CDW layer and U is the mean along-slope velocity that is assumed constant in this analysis. In this way, longer mixing lengths are associated with higher eddy diffusivities and increased eddy stirring along isopycnals. L_{mix} and κ are calculated in each of the longitudinal sections and averaged across longitudes considered in the East Antarctic mean. Additionally, L_{mix} and κ are compared in composite means in eddying and noneddying regions (i.e., regions above and below the σ_{spice} threshold). The standard deviation of κ across longitudes is taken as a measure of the uncertainty in the estimate and is used to set an upper and lower bound on transport estimates.

Results of the seal-based analysis are compared with the direction of eddy transport inferred from the density-layer thickness changes along each of the ship-based hydrography lines. That is, $\bar{h}_y$ is calculated in the CDW and AASW layers for each occupation and then averaged along each of the four transects, where y is the distance between CTD stations. Standard errors of the means are calculated as $\sigma_{h_y}/\sqrt{N_{\text{years}}}$, where σ_{h_y} is the standard deviation of density-layer thickness gradients among occupations and N_{years} is the number of occupations.

4. Results

4.1. Along-Slope Hydrographic Variability

The midslope mean temperature, salinity, and spice (where the averaging is done between the 1,800- and 2,200-m isobaths) vary along-slope (Figure 2, left column). The mean temperature at 500 dbar, for example, varies by more than 1 °C between 80°E and 100°E. The interface between the AASW and CDW layer ($\bar{\rho} = 1,027.76$ kg/m^3, black line) roughly tracks the $\bar{T} = 0$ °C isotherm. Above the $\bar{T} = 0$ °C isotherm, cooler and fresher AASW is found sitting atop the CDW layer. The mean depth of the 0 °C isotherm varies by a few hundred meters along the East Antarctic slope between about 200 and 700 dbar. Similar patterns of along-slope variability are found if all profiles taken between the 1,000- and 3,000-m isobaths are included in the average (compare left and center columns of Figure 2). Thus, the along-slope structure of CDW intrusions

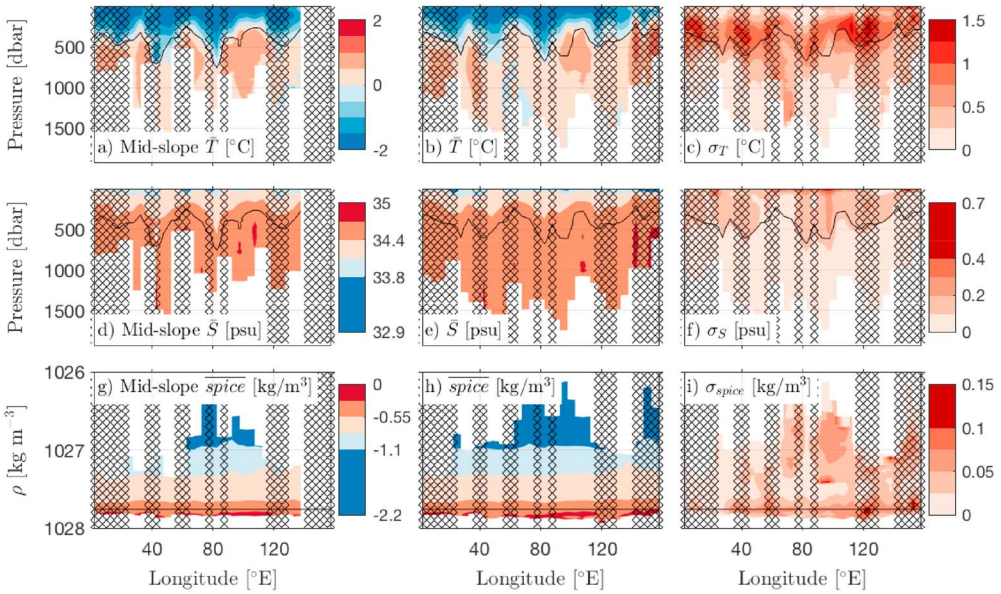

Figure 2. Along-slope hydrography. (a, d) Midslope mean temperature and salinity, that is, averaged over the 1,800- to 2,200-m isobaths, as a function of pressure within 5° longitude bins. (b, e) Cross-slope mean temperature and salinity, that is, averaged over the 1,000- to 3,000-m isobaths, as a function of pressure within 5° longitude bins. (c, f) Cross-slope temperature and salinity standard deviation of profiles taken over the 1,000- to 3,000-m isobaths as a function of pressure within 5° longitude bins. (g–i) Midslope mean, cross-slope mean, and standard deviation of spice as a function of surface-referenced potential density. In all panels, the isopycnal at the interface between the AASW and CDW layers is shown as a black line. Longitudes with hatching over top are excluded from the analysis due data sparsity.

is likely due to physical processes controlling cross-slope transport of CDW rather than sampling biases on the upper and lower slope.

The standard deviation of properties in each 5° longitude bin (using all profiles in the longitude bin) shows regions of heightened hydrographic variability (Figures 2c and 2f). Temperature variability (σ_T) is largest near 300 dbar, generally just above the $\bar{T} = 0$ °C isotherm, whereas salinity variability (σ_S) is concentrated at the surface. Along-isopycnal spice standard deviation largely matches the pattern of σ_T, with the highest variance near the interface between CDW and AASW (Figure 2i). A spice standard deviation threshold of $\sigma_{\text{spice}} = 0.06$ kg/m^3 at 1,027.77 kg/m^3 is taken to define regions of high and low spice variability (high-variability regions denoted by black outlined circles in Figure 1b). Spice variability exceeds this threshold for 35% of the longitudes considered from the East Antarctic slope, that is, 25° of longitude fall in eddying regions. It can be noted that the spice standard deviation at 1,027.77 kg/m^3 is not directly related to the number of profiles in a given 5° longitude bin, suggesting that σ_{spice} represents regional hydrographic variability rather than profile density.

4.2. Mean Cross-Slope Eddy Transport

The East Antarctic cross-slope mean temperature and salinity fields show cold, fresh AASW above and farther upslope than warm, salty CDW (Figures 3a and 3b). The thickness of the AASW layer increases toward the shelf break, associated with onshore deepening of isotherms and isohalines in the upper water column (roughly 100–700 dbar). The interface between the AASW and CDW layers ($\bar{\rho} = 1,027.76$ kg/m^3) lies roughly on the $\bar{T} = 0$ °C isotherm, albeit deeper above the lower slope and shallower above the upper slope. The interface deepens by 125 m across the slope, from about 375 dbar above the lower slope to 500 dbar at the shelf break. Colder waters, with $\bar{T} < 0$ °C, also appear below the CDW layer between 1,000 and 1,700 dbar and above isobaths shallower than 2,000 m, possibly indicating the presence of dense bottom water (not shown). Yet, the lack of deep-reaching profiles implies tenuous statistics at these depths. We therefore focus on cross-slope CDW and AASW transport by eddies in the upper part of the water column and only present results in the upper 1,000 dbar.

Cross-slope gradients in the mean thickness of density layers indicate onshore transport of warm, salty water around 500 dbar and offshore transport of cold, fresh water in the upper ocean (Figure 3c). The denser CDW

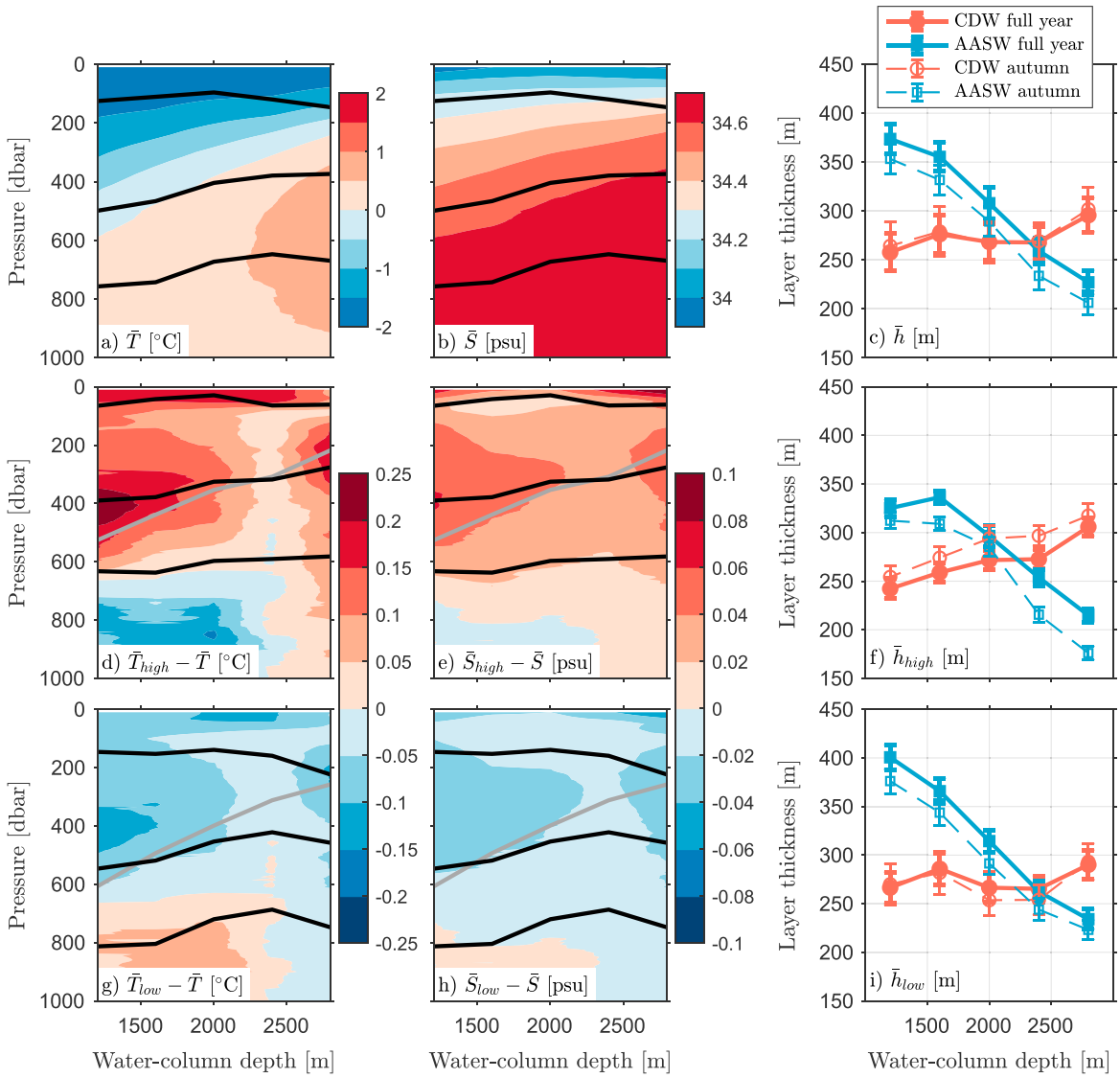

Figure 3. Across-slope mean (a) temperature, (b) salinity, and (c) density-layer thickness from the East Antarctic continental slope and across-slope mean (d, e, g, and h) hydrography anomalies relative to East Antarctic mean and (f, i) density-layer thicknesses in high spice variability and low spice variability regions. (c, f, and i) Red circles represent the thickness of the CDW layer; blue squares represent thickness of AASW layer. Thick solid lines with filled markers represent layer thicknesses calculated using data throughout the year and thin dashed lines with open markers represent layer thicknesses calculated using data from autumn (March–May). (a, b, d, e, g, and h) Mean depth of the interface between the CDW and AASW layers ($\bar{\rho}$ = 1027.76 kg/m^3) is represented by middle black line for each regional average. The mean depth of the top and bottom of the AASW and CDW layers, respectively, are represented by the upper and lower black lines, where the depths are determined by the mean layer thicknesses. The gray lines illustrate the depth of the mean T = 0 °C isotherms in (d, e) high and (g, h) low variability regions. CDW = Circumpolar Deep Water; AASW = Antarctic Surface Water.

layer ($\bar{\rho}$ = 1,027.76–1,027.82 kg/m^3) shows onshore thinning of about 40 m across the slope. The lighter AASW layer ($\bar{\rho}$ = 1,027.44–1,027.76 kg/m^3) shows steady offshore thinning by almost 150 m. Standard errors on the $\bar{\rho}$-layer thicknesses are 16–19 m for the CDW layer and 12–16 m for the AASW layer in each isobath range (see section 3 for details of error calculation), making eddy transports statistically significant in both layers. This onshore CDW transport and offshore AASW transport is consistent with an overturning of the upper layers, where there is an influx of CDW to the shelf break and an export of AASW away from the shelf. The eddy-induced overturning remains similar whether considering all available data or only data from the best sampled months (March–May; Figure 3c), albeit the onshore CDW transport is statistically insignificant during the autumn months as the standard errors are larger.

The magnitude of eddy transport is calculated as $\psi_{\text{eddy}} = \overline{v'h'} = -\kappa \bar{h}_y$ in the CDW layer, where $\kappa = L_{\text{mix}} U$. Here, we assume a constant $U = 0.017$ m/s, the mean velocity near 500 dbar in a current-meter mooring array on the East Antarctic slope at 113°E (Peña-Molino et al., 2016) and a slope width of 100 km. This results in an average $\bar{L}_{\text{mix}}$ of 56 km. The mean eddy diffusivity on the East Antarctic slope is $\kappa = 950 \pm 400$ m^2/s, where the uncertainty represents the standard deviation among longitudes. This translates to $\psi_{eddy} = (0.6 \pm 0.3)$ m^2/s, equivalent to 3 Sv of onshore CDW transport by eddies over the 70° of longitude (roughly 5,000 km) considered in this study. Note that a slope width of 100 km is assumed when calculating cross-slope gradients; however, it becomes irrelevant in the ψ_{eddy} calculation as it cancels between $\bar{h}_y$ and L_{mix}.

4.3. Along-Slope Variability in Eddy Transport

The signal of eddy-induced overturning across the East Antarctic slope—onshore transport of deeper CDW and offshore transport of shallower AASW—is only apparent in the regions of high hydrographic variability (Figures 3f and 3i). High-variability regions are defined as longitudinal bins with increased spice variability in the CDW layer, that is, $\sigma_{\text{spice}} \geq 0.06$ kg/m^3 along the 1,027.77-kg/m^3 isopycnal. In these regions, the denser CDW layer thins by about 65 m in the onshore direction, with standard errors of 9–10 m, and the lighter AASW layer thins by about 100 m in the offshore direction, with standard errors of 7–11 m (Figure 3f). In low variability regions, there is no significant onshore thinning of the CDW layer and the AASW thins by about 150 m in the offshore direction, with standard errors of 10–13 m (Figure 3i). As found for the mean fields, the results are similar if only March–May profiles are analyzed (Figure 3, right column).

The magnitude of eddy diffusivity in the CDW layer, again assuming $U = 0.017$ m/s and a slope width of 100 km, is approximately $\kappa_{\text{high}} = 850 \pm 400$ m^2/s in high-variability regions compared to $\kappa_{\text{low}} = 1000 \pm 500$ m^2/s in low-variability regions. While the spice variability (σ_{spice}) is higher in the eddying regions, the mean spice gradient magnitude along isopycnals is greater in low-variability regions. The resulting mixing lengths are roughly equal, with $L_{\text{mix}} = 50$ km in high-variability regions compared to $L_{\text{mix}} = 60$ km in low variability regions. Yet, the large standard deviations among κ values at different longitudes makes κ_{high} and κ_{low} statistically indistinguishable from each other and from the East Antarctic mean value. Low variability regions have insignificant eddy transport of CDW, as $\bar{h}_y$ is insignificant in those regions. In high-variability regions, $\psi_{\text{eddy}} = 0.8 \pm 0.4$ m^2/s, equivalent to about 0.8 Sv of CDW onshore across the approximately 1,000 km of slope.

Consistent with onshore eddy transport of CDW and eddy-induced overturning, high-variability regions have spicier—warmer and saltier—waters in the upper part of the water column (above about 700 dbar) than those in low-variability regions (Figures 3d, 3e, 3g, and 3h). Temperature and salinity anomalies of ±0.2–0.25 °C and ±0.06 psu, respectively, relative to the mean over the East Antarctic slope, are largest near 400 dbar and are generally concentrated on the upper slope (above the 1,000- to 1,400-m isobaths). Moreover, the 0 °C isotherm is 80 m shallower on the onshore side of the slope in the high-variability regions compared to low-variability regions. These results indicate a greater availability of CDW, that is, an increase in the heat and salt reservoirs, at the shelf break in these eddying regions due to cross-slope eddy transport.

Cross-slope density-layer thickness changes from ship-based hydrography lines (see Figures 1a and 1b for transect locations) show similar along-slope variability in the direction of eddy transport inferred from seal-based hydrography. The AASW layer ($\bar{\rho} = 1,027.44$–$1,027.76$ kg/m^3) shows significant offshore eddy transport at all of the transects, with the exception of I6S where the offshore transport is not significantly different from zero. Mean offshore thinning rates of 0.4–1.1 m/km are found along each of the four lines (not shown). This is consistent with the seal-based density-layer thickness analysis that found eddy transport of AASW in the offshore direction, independent of regional spice variability (Figure 3, right column). Further, if the width of the slope is assumed to be 100 km, the thinning rates from the seal-based analysis of 1–1.5 m/km are of similar, albeit slightly larger, magnitude as those found along repeat hydrography lines.

The CDW layer ($\bar{\rho} = 1,027.76$–$1,027.82$ kg/m^3) also shows agreement in the direction of eddy transport between ship- and seal-based hydrography, except along I9S (not shown). We find onshore transport of CDW along SR3 ($\bar{h}_y = 1.4 \pm 0.4$ m/km), which is adjacent to a high-variability region. Along I6S and I8S, transects falling in and adjacent to low variability regions, respectively, the ship-based hydrography show statistically insignificant layer thickness changes. There is a discrepancy along I9S, where the ship-based hydrography

shows significant onshore transport of CDW ($\bar{h}_y = 1.3 \pm 0.6$ m/km) while the seal-based analysis deems it a low variability region with insignificant transport of CDW.

5. Discussion

The along-slope variability of cross-slope eddy transport and overturning, inferred from layer thickness changes of different density classes, reveals the spatial pattern of eddy-driven heat and salt delivery to the continental shelf break. Stronger eddy transport of CDW results in warmer and saltier water at the shelf break (Figures 3d, 3e, 3g, and 3h). This reservoir of heat and salt is available to be transferred across the shelf break by a variety of processes (Stewart et al., 2018), with potential to enhance melt of ice shelves and influence stratification and water mass formation. In fact, modified CDW has been observed intruding under ice shelves in East Antarctica (Silvano et al., 2016, 2017) and driving rapid basal melting (Rintoul et al., 2016).

Eddies are not the only mechanism for onshore CDW transport; tides, coastal-trapped waves, and winds also drive cross-slope exchange. The relative importance of each mechanism changes regionally and with water column depth (Stewart et al., 2018). Here, eddy transport is strongest in deeper water (above the 2,200- to 3,000-m isobaths; Figure 3f). This is consistent with ultrahigh resolution model results, where eddies transport heat across the lower slope (above the 1,500-m isobath and deeper) and tidal fluxes become important for heat transport across the shelf break (Stewart et al., 2018). From this perspective, the slope and shelf break act as two distinct gateways for poleward heat transport, and there is a hand-off of heat between mechanisms during the poleward transit.

Thompson et al. (2014) use scaling arguments, where $\psi_{\text{eddy}} = -\kappa \bar{h}_y$ and $\psi_{\text{wind}} = \tau/(\rho_0 f)$, on high-resolution glider data and find the eddy-driven overturning to be about half the magnitude of wind-driven overturning on the West Antarctica Peninsula in the northwest Weddell Sea. Thus, the local eddy-induced transport was found to be a key mechanism for cross-slope exchange. The observations presented here, assuming a slope width of 100 km, show values of $\bar{h}_y$ more than an order of magnitude smaller than those found by Thompson et al. (2014). The averaging done in this analysis results in significantly smoother fields than the glider observations, such that the magnitude of layer thickness changes is not expected to be as large. Moreover, the coarseness of the averaged fields here is reflected in the large values of κ (more than an order of magnitude greater than the value of 14 m^2/s used by Thompson et al. (2014)). Thus, the resulting eddy transports are more than 5 times greater than that found by Thompson et al. (2014), with $\psi_{\text{eddy}} = 0.8$ m^2/s in the eddying regions here compared with $\psi_{\text{eddy}} = 0.14$ m^2/s inferred from their glider data.

Taking a range of climatological wind stress magnitudes of $\tau = 0.05$–0.2 N/m^2 over the East Antarctic slope (Large & Yeager, 2009), we estimate the relative strength of the eddy-induced overturning. With our nominal value of $\kappa = 900$ m^2/s, we find $\psi_{\text{eddy}}/\psi_{\text{wind}}$ ranges from about 0.5 for $\tau = 0.2$ N/m^2 to 2.2 for $\tau = 0.05$ N/m^2. Depending on local values of τ and given the uncertainty in the estimates of κ, the eddy-driven overturning could be as small as 20% of the magnitude or as large as triple the magnitude of the wind-driven overturning. That is, for $\tau = 0.2$ N/m^2 and $\kappa = 500$ m^2/s, $\psi_{\text{eddy}}/\psi_{\text{wind}} = 0.2$; for $\tau = 0.05$ N/m^2 and $\kappa = 1,300$ m^2/s, the eddy-driven overturning is almost 3 times as strong as the wind-driven overturning. The large uncertainties here reflect the uncertainty in the observations of both ψ_{eddy} and ψ_{wind}. More in situ observations are needed to further constrain them.

6. Conclusion

This work provides an observational estimate of the eddy contribution to cross-slope transport in East Antarctica (between the 1,000- and 3,000-m isobaths and between 0°E and 160°E). Changes in the mean thickness of density layers indicate onshore eddy transport of CDW and offshore transport of AASW. However, eddy transport is not uniform along the continental slope. Onshore eddy transport of CDW is concentrated in regions of high spice variability, while low-variability regions have insignificant CDW transport by eddies. Strong eddy transport results in warm and salty anomalies at the shelf break. This reservoir of heat and salt can be transferred to the continental shelf by tides, topographic waves, wind-driven flows, and eddies. In this way, cross-slope eddy transport can facilitate transport of heat and salt from the open ocean to the continental shelf in particular regions, with implications for the ocean-atmosphere-cryosphere interactions that regulate melt of ice shelves (hence ice sheet mass loss and sea level rise) and formation of dense shelf water (hence the global overturning circulation).

Acknowledgments
This research was supported by the Centre for Southern Hemisphere Oceans Research (CSHOR), a partnership between the Commonwealth Scientific and Industrial Research Organisation (CSIRO) and the Qingdao National Laboratory for Marine Science, as well as the Australian Antarctic Program and Australia's Integrated Marine Observing System. S. R. R. was supported by the Australian Government's Cooperative Research Centre program through the Antarctic Climate and Ecosystems Cooperative Research Centre and by the Australian Government's National Environmental Science Programme. M. H. E. was supported by the Australian Research Council (Grants DP190100494 and CE17010023). The seal-based hydrography were collected and made freely available by the International MEOP Consortium and the national programs that contribute to it (http://www.meop.net). The ship-based hydrography used in this study are publicly available from the Clivar and Carbon Hydrographic Data Office (CCHDO; http://cchdo.ucsd.edu), with the exception of SR3 occupations in 2013 and 2015, which are available on the Australian Antarctic Data Centre (https://data.aad.gov.au/aadc/) under voyage names ta1302 and au1402, respectively. The authors are grateful to Andy Thompson for his valuable insight; we also thank two anonymous reviewers for constructive comments on the manuscript.

References

Bindoff, N. L., Rosenberg, M. A., & Warner, M. J. (2000). On the circulation and water masses over the Antarctic continental slope and rise between 80 and 150 E. *Deep Sea Research II: Topical Studies in Oceanography*, *47*(12-13), 2299–2326. https://doi.org/10.1016/S0967-0645(00)00038-2

Boehme, L., Lovell, P., Biuw, M., Roquet, F., Nicholson, J., Thorpe, S. E., et al. (2009). Technical note: Animal-borne CTD-satellite relay data loggers for real-time oceanographic data collection. *Ocean Science*, *5*(4), 685–695. https://doi.org/10.5194/os-5-685-2009

Flament, T., & Rémy, F. (2012). Dynamic thinning of Antarctic glaciers from along-track repeat radar altimetry. *Journal of Glaciology*, *58*(211), 830–840. https://doi.org/10.3189/2012JoG11J118

Fretwell, P., Pritchard, H. D., Vaughan, D. G., Bamber, J., Barrand, N., Bell, R., et al. (2013). Bedmap2: Improved ice bed, surface and thickness datasets for Antarctica. *The Cryosphere*, *7*, 375–393. https://doi.org/10.5194/tc-7-375-2013

Harig, C., & Simons, F. J. (2015). Accelerated West Antarctic ice mass loss continues to outpace East Antarctic gains. *Earth and Planetary Science Letters*, *415*, 134–141. https://doi.org/10.1016/j.epsl.2015.01.029

Heywood, K. J., Schmidtko, S., Heuzé, C., Kaiser, J., Jickells, T. D., Queste, B. Y., et al. (2014). Ocean processes at the Antarctic continental slope. *Philosophical Transactions of the Royal Society A*, *372*(2019), 20130047. https://doi.org/10.1098/rsta.2013.0047

IMBIE (2018). Mass balance of the Antarctic Ice Sheet from 1992 to 2017. *Nature*, *558*, 219–222. https://doi.org/10.1038/s41586-018-0179-y

Karsten, R. H., & Marshall, J. (2002). Constructing the residual circulation of the ACC from observations. *Journal of Physical Oceanography*, *32*(12), 3315–3327. https://doi.org/10.1175/1520-0485(2002)032<3315:CTRCOT>2.0.CO;2

Large, W. G., & Yeager, S. G. (2009). The global climatology of an interannually varying air-sea flux dataset. *Climate Dynamics*, *33*, 341–364. https://doi.org/10.1007/s00382-008-0441-3

Li, X., Rignot, E., Mouginot, J., & Scheuchl, B. (2015). Grounding line retreat of Totten Glacier, East Antarctica, 1996 to 2013. *Geophysical Research Letters*, *42*, 8049–8056. https://doi.org/10.1002/2015GL065701

Marshall, J., & Radko, T. (2003). Residual-mean solutions for the Antarctic Circumpolar Current and its associated overturning circulation. *Journal of Physical Oceanography*, *33*(11), 2341. https://doi.org/10.1175/1520-0485(2003)033<2341:RSFTAC>2.0.CO;2

McDougall, T. J., & Barker, P. M. (2011). Getting started with TEOS-10 and the Gibbs Seawater (GSW) Oceanographic Toolbox. *SCOR/IAPSO WG127*, *ISBN: 978-0-646-55621-5*, 28.

McDougall, T. J., & Krzysik, O. A. (2015). Spiciness. *Journal of Marine Research*, *73*(5), 141–152. https://doi.org/10.1357/002224015816665589

Meijers, A. J. S., Klocker, A., Bindoff, N. L., Williams, G. D., & Marsland, S. J. (2010). The circulation and water masses of the Antarctic shelf and continental slope between 30 and 80E. *Deep Sea Research II: Topical Studies in Oceanography*, *57*(9-10), 723–737. https://doi.org/10.1016/j.dsr2.2009.04.019

Munk, W. (1981). The evolution of physical oceanography. In B. A. Warren & C. Wunsch (Eds.), *Chap. Internal wave and small-scale processes*. Cambridge, MA: MIT Press.

National Geophysical Data Center (2006). 2-minute Gridded Global Relief Data (ETOPO2) v2 (Tech. Rep.): National Geophysical Data Center, NOAA. https://doi.org/10.7289/V5J1012Q

Naveira Garabato, A. C., Ferrari, R., & Polzin, K. L. (2011). Eddy stirring in the Southern Ocean. *Journal of Geophysical Research*, *116*, C09019. https://doi.org/10.1029/2010JC006818

Nøst, O. A., Biuw, M., Tverberg, V., Lydersen, C., Hattermann, T., Zhou, Q., et al. (2011). Eddy overturning of the Antarctic Slope Front controls glacial melting in the Eastern Weddell Sea. *Journal of Geophysical Research*, *116*, C11014. https://doi.org/10.1029/2011JC006965

Palóczy, A., Gille, S. T., & McClean, J. L. (2018). Oceanic heat delivery to the Antartic continental shelf: Large-Scale, low-frequency variability. *Journal of Geophysical Research: Oceans*, *123*, 7678–7701. https://doi.org/10.1029/2018JC014345

Paolo, F. S., Fricker, H. A., & Padman, L. (2015). Volume loss from Antarctic ice shelves in accelerating. *Science*, *348*(6232), 327–331. https://doi.org/10.1126/science.aaa0940

Peña-Molino, B., McCartney, M. A., & Rintoul, S. R. (2016). Direct observations of the Antarctic Slope Current transport at 113E. *Journal of Geophysical Research: Oceans*, *121*, 7390–7407. https://doi.org/10.1002/2015JC011594

Pritchard, H. D., Arthern, R. J., Vaughan, D. G., & Edwards, L. A. (2009). Extensive dynamic thinning on the margins of the Greenland and Antarctic ice sheets. *Nature*, *461*, 971–975. https://doi.org/10.1038/nature08471

Rintoul, S. R., Silvano, A., Peña-Molino, B., van Wijk, E., Rosenberg, M. A., Greenbaum, J. S., & Blankenship, D. D. (2016). Ocean heat drives rapid basal melt of the Totten Ice Shelf. *Science Advances*, *2*(12), e1601610. https://doi.org/10.1126/sciadv.1601610

Roquet, F., Guinet, C., Charrassin, J.-B., Costa, D. P., Kovacs, K. M., Lydersen, C., et al. (2018). MEOP-CTD in-situ data collection: A Southern Ocean Marine-mammals calibrated sea water temperatures and salinities observations (Tech. Rep.): SEANOE. https://doi.org/10.17882/45461

Roquet, F., Williams, G. D., Hindell, M. A., Harcourt, R., McMahon, C., Guinet, C., et al. (2014). A Southern Indian Ocean database of hydrographic profiles obtained with instrumented elephant seals. *Scientific Data*, *1*, 140028. https://doi.org/10.1038/sdata.2014.28

Siegelman, L., Roquet, F., Mensah, V., Rivière, P., Pauthenet, E., Picard, B., & Guinet, C. (2019). Correction and accuracy of high- and low-resolution CTD data from animal-borne instruments. *Journal of Atmospheric and Oceanic Technology*, *36*, 745–760. https://doi.org/10.1175/JTECH-D-18-0170.1

Silvano, A., Rintoul, S. R., & Herraiz-Borreguero, L. (2016). Ocean-ice shelf interaction in East Antarctica. *Oceanography*, *29*(4), 130–143. https://doi.org/10.5670/oceanog.2016.105

Silvano, A., Rintoul, S. R., Peña-Molino, B., & Williams, G. D. (2017). Distribution of water masses and meltwater on the continental shelf near the Totten and Moscow University ice shelves. *Journal of Geophysical Research: Oceans*, *122*, 2050–2068. https://doi.org/10.1002/2016JC012115

Stewart, A. L., Klocker, A., & Menemenlis, D. (2018). Circum-Antarctic shoreward heat transport derived from an eddy- and tide-resolving simulation. *Geophysical Research Letters*, *45*, 834–845. https://doi.org/10.1002/2017GL075677

Stommel, H. (1961). On the cause of the temperature-salinity curve in the ocean. *Proceedings of the National Academy of Science*, *48*, 764–766. https://doi.org/10.1073/pnas.48.5.764

Thompson, A. F., Heywood, K. J., Schmidtko, S., & Stewart, A. L. (2014). Eddy transport as a key component of the Antarctic overturning circulation. *Nature Geoscience*, *7*(12), 879–884. https://doi.org/10.1038/ngeo2289

Thompson, A. F., Stewart, A. L., Spence, P., & Heywood, K. J. (2018). The Antarctic Slope Current in a changing climate. *Reviews of Geophysics*, *56*, 741–770. https://doi.org/10.1029/2018RG000624

Treasure, A. M., Roquet, F., Ansorge, I. J., Bester, M. N., Boehme, L., Bornemann, H., et al. (2017). Marine mammals exploring the oceans pole to pole: A review of the MEOP Consortium. *Oceanography*, *30*(2), 132–138. https://doi.org/10.5670/oceanog.2017.234

Veronis, G. (1972). On the properties of seawater defined by temperature, salinity and pressure. *Journal of Marine Research*, *30*, 227–255.

Whitworth, T. III, Orsi, A. H., Kim, S.-J., Nowlin, W. D. Jr., & Locarnini, R. A. (1998). Water masses and mixing near the Antarctic Slope Front. *Ocean, Ice, and Atmosphere: Interactions at the Antarctic Continental Margin*, *75*, 1–27. https://doi.org/10.1029/AR075p0001